05

Atomic force microscopy of nanostructured multicomponent alloys (Tb,Dy,Gd)Co_2

© I.S. Tereshina,[1] T.P. Kaminskaya,[1] A.A. Aleroev,[1,2] A.Yu. Karpenkov[3]

[1] Moscow State University,
119991 Moscow, Russia
[2]Grozny State Oil Technical University,
364051 Grozny, Russia
[3]Tver State University,
170100 Tver, Russia
e-mail: irina_tereshina@mail.ru; tereshina@physics.msu.ru

Received May 28, 2025
Revised June 30, 2025
Accepted September 5, 2025

The nanostructured state of multicomponent (Tb,Dy,Gd)Co_2 alloys was studied using atomic force microscopy. Ribbon-shaped samples with a distinct directional structure were obtained by rapid melt crystallization on a rotating copper disk. Ribbon cleavages, as well as the contact and free surfaces of the ribbon samples, were examined. The features of the topography, structure, defects on both surfaces, and the morphology of nanograins were determined for two rapidly quenched samples of different compositions: $Tb_{0.2}Dy_{0.5}Gd_{0.3}Co_2$ and $Tb_{0.8}Dy_{0.1}Gd_{0.1}Co_2$. Using the atomic force microscopy results, the increase in magnetostrictive properties of the rapidly quenched samples compared to the original ones was interpreted. It was noted that the high performance of the alloys is due to the volume effect (associated with the dependence of the exchange integrals on the unit cell volume).

Keywords: Rare earth intermetallics, Laves phases, rapid quenching, nanostructured state, nanograins, atomic force microscopy, magnetostriction, volumetric effect.

DOI: 10.61011/TP.2026.01.62846.132-25

Introduction

Compounds with the RCo_2 general formula (here R is a rare-earth metal (REM)) are items with magnetic properties that are exceptionally important in terms of practice, i.e. magnetostrictive and magnetothermal (magnetocaloric) properties [1–9]. It stimulates, on the one hand, comprehensive investigation of their properties using the most modern equipment created by scientists and engineers and, on the other hand, improvement of various technological processes as well as instruments and devices, in which these compositions are used.

Having a structure of the Laves phases, the RCo_2 compounds demonstrate a wide spectrum of functional properties in a quite large temperature range from 4 to 400 K in a dependence on a type of the used rare-earth metal (in a row from lanthanum to lutetium). The properties of the RCo_2 double compounds are quite well studied [2,3]. Therefore, large attention is now paid to the properties of multi-component compounds. These compounds are produced by means of substitution atoms [10]: usually, substitutions are possible both in a cobalt sublattice as well as in a sublattice of the rare-earth metal with preservation of a crystal structure.

Recently, especially important are comparative studies of properties of compounds of the RCo_2 type, which are produced in a various structural state from mono-, poly- to nano-crystalline (nanostructured) one [1,11–13]. These studies are today conducted only fragmentarily and there is often no comprehensive approach to studying their properties.

One of the most common methods of forming the nanocrystalline (nanostructured) state for the rare-earth intermetallic compounds based on 3*d*-transition metals (such cobalt and iron) is a method of rapid melt quenching. After the rapid quenching procedure, the alloy properties (mechanical, magnetic, magnetostrictive and magnetothermal) significantly change [14–16]. A sample shape is also changes: fast melt crystallization results in tape samples on a copper disk rotating at a pre-defined rotational speed. At the same time, a quenching rate is an important parameter. Along with the crystal phase, the tape samples usually exhibit formation of an amorphous phase as well. A ratio of the crystal and the amorphous phase as well as sizes of forming grains can vary within quite wide limits in a dependence on the disk rotational speed. The tape-shaped samples are demanded in practice and convenient for scientific studies using various modern equipment. Thus, using tape as well as film samples instead of cast ones makes it possible to miniaturize the instruments and devices [15]. When using the R–Co(Fe) samples as working bodies of refrigerators, the tape samples allow removing heat

much faster and, therefore, they can increase refrigerator efficiency [15].

A method of atomic force microscopy (AFM) that is developed and widely used in recent decades can be applied to study both a state of the (contact and free) surface of the tape samples as well as a cross section of the tapes [17,18]. Studying a surface topography by means of AFM makes it possible to reproduce a three-dimensional structure of the sample surface with spatial resolution of about 10 nm or less and to detect various structural specific features, including when varying the composition of the studied samples. At the same time, it is extremely important to find a relation of structural and functional properties of the samples.

Taking into account the foregoing, the present study is aimed at demonstrating efficiency of the AFM method for studying the nanostructured multi-component (Tb,Dy,Gd)Co_2 alloys with the structure of the Laves phases, which are produced as a result of rapid sample quenching as well as at revealing an interrelation between their structural and magnetostrictive properties. Objects of research were the two compositions $Tb_{0.2}Dy_{0.5}Gd_{0.3}Co_2$ and $Tb_{0.8}Dy_{0.1}Gd_{0.1}Co_2$ with a various content of highly-anisotropic and isotropic trivalent ions of the rare-earth metals, namely, terbium, dysprosium and gadolinium. All the used rare-earth metals belong to a group of heavy ones, while the (Tb,Dy,Gd)Co_2 compounds themselves are ferrimagnetics.

High values of magnetostriction in these samples can be observed both within the low temperatures (near the absolute-zero temperature) as well as around the Curie temperature — of a magnetic phase transition from the ferrimagnetic into paramagnetic state. In the latter case, a value of volume magnetostriction is especially important. Indeed, the value of the Curie temperature depends on exchange interactions inside separate sublattices (of cobalt and the rare-earth metal) as well as on exchange interaction between the sublattices. Around the Curie temperature, volume magnetostriction that is large in value occurs due to a dependence of integrals of exchange interactions on the distances between ions in the pairs Co–Co, Co–R, R–R and it is exchange magnetostriction, actually.

In order to achieve the aim set herein, we have studied specific features of the topography and structure of the surfaces and cleavages on a micro- and nano-level for the two produced tape samples of the different composition $Tb_{0.2}Dy_{0.5}Gd_{0.3}Co_2$ and $Tb_{0.8}Dy_{0.1}Gd_{0.1}Co_2$. The AFM results were used to interpret the change of the magnetostrictive characteristics of rapidly-quenched samples as compared to the initial cast ones around the Curie temperature.

1. Experimental procedure

The cast samples $Tb_{0.2}Dy_{0.5}Gd_{0.3}Co_2$ and $Tb_{0.8}Dy_{0.1}Gd_{0.1}Co_2$ were prepared by a known technology using arc vacuum melting and subsequent homogenizing annealing. All the details of producing the initial cast samples and their certification are previously explained in detail in the study [19]. The cast samples were produced in the polycrystalline state as disks. In order to produce the nanostructured samples as tapes, the ingots were remelt and the melt was crystallized on the rotating copper disk. A linear speed of the rotating disk on the surface in a place of contact of the melt was 15 m/s. The selected compositions ($Tb_{0.2}Dy_{0.5}Gd_{0.3}Co_2$ and $Tb_{0.8}Dy_{0.1}Gd_{0.1}Co_2$) and a process mode of producing the tape samples completely excluded their phase delamination, which quite often takes place during a procedure of rapid melt quenching. The phase composition and parameters of the crystal lattice of the rapidly-quenched samples were determined by performing studies by an X-ray diffraction analysis (XDA) method at the room temperature.

XDA of the powder samples was performed in a diffractometer DRON-7.0. An X-ray tube with CuK_α-radiation ($\lambda = 0.1540598$ nm) was used at an X-ray source. The parameters of the lattice cell were determined by reflections in a range of the angles $2\theta = 15 - 105^\circ$. Experimental X-ray spectra were analyzed using the PowderCell software. The software uses a method of full-profile Rietveld analysis, which describes a profile of the entire experimental pattern of scattering and comparatively analyzes with a theoretical X-ray diffraction pattern. The diffraction patterns were analyzed by means of a full spectrum fitting procedure in order to determine the structural properties. Each structural model was refined to convergence and the best results were chosen according to the coefficient of concordance and stability of refinement. Since the rare-earth RCo_2 intermetallics crystallized into a cubic structure of the $MgCu_2$ type (the structure of the type of the Laves phases (C15), the space group $Fd\bar{3}m$ №227), the theoretical spectra were constructed using ion coordinates in the cell, which are given in Table 1.

The topography of the surface structure of the studied samples $Tb_{0.2}Dy_{0.5}Gd_{0.3}Co_2$ and $Tb_{0.8}Dy_{0.1}Gd_{0.1}Co_2$ was studied using the scanning probe microscope SMENA-A, the platform „Solver“ (NT-MDT, RF, Zelenograd). The samples were studied at the room temperature in semi-contact and contact modes using standard silicon cantilevers HA_NC ETALON with resonance frequencies 140 – 235 kHz, NSG 03 with resonance frequencies from 47 to 150 kHz, a tip rounding radius of 10 nm, a power constant 0.35 – 6.1 N/m and cantilevers DCP_IN with the resonance frequencies 500 – 1000 kHz, the tip rounding radius of 25 nm and the power constant 100 – 600 N/m for operation in the contact mode. The obtained AFM images were processed using the NOVA software.

The Curie temperature of the studies alloys was determined by means of thermomagnetic analysis (TMA). Magnetostrictive strains were measured using a tensometric method. The experiment was conducted using strain gauges made of wire of the diameter of 30 μm, which did not exhibit galvanomagnetic effects. A base of the strain gauge was 3 mm, resistance was 100 Ω, and a gauge factor was

Table 1. Ion coordinates in a cell of the RCo_2 compounds (in fractions of lattice cell vectors)

Ion	Wyckoff position (Wyckoff)	*x*	*y*	*z*	Occupancy
Compound $Tb_{0.2}Dy_{0.5}Gd_{0.3}Co_2$					
T	8b	1/4	1/4	1/4	0.2
Dy	8b	1/4	1/4	1/4	0.5
Gd	8b	1/4	1/4	1/4	0.3
Co	16c	7/8	7/8	7/8	1
Compound $Tb_{0.8}Dy_{0.1}Gd_{0.1}Co_2$					
Tb	8a	0	0	0	0.8
Dy	8a	0	0	0	0.1
Gd	8a	0	0	0	0.1
Co	16d	3/8	7/8	1/8	1

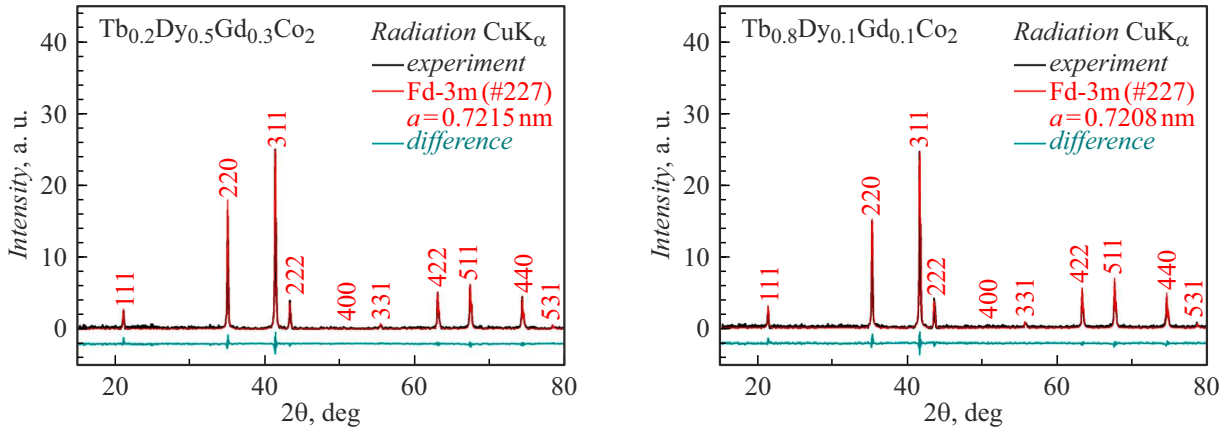

Figure 1. Diffraction patterns of the powder samples $Tb_{0.2}Dy_{0.5}Gd_{0.3}Co_2$ and $Tb_{0.8}Dy_{0.1}Gd_{0.1}Co_2$, obtained at the room temperature. The black curves mark experimental spectra, the red curves mark theoretically-calculated diffraction patterns obtained by the Rietveld method and the green curves mark difference curves of the diffraction patterns. Each compound is provided with Miller indices of reflections that are the strongest in terms of intensity.

$k = 2.15$. One of the strain gauges (the working one) was glued to the sample, while the other one was glued to a thin quartz plate and used as a compensation element. The gauges were selected so that their resistance was not different by more than 0.1 % in order to provide high accuracy of measurements. Both the strain gauges were connected to a Wheatstone bridge simultaneously with two resistance boxes. The circuit was calibrated by means of a reference resistance of 0.1 Ω (the OKS-3 type), which was included into a bridge arm in series with a resistance of the working strain gauge. A bridge disbalance signal was recorded by a digital voltmeter V7-21A (a working limit is 100 pA). The length change was calculated by the formula

$$\lambda = \frac{R_{\text{ref}}}{kR_0\varphi_{\text{ref}}}\varphi_0.$$

Here k is the gauge factor, R_0 is the resistance of the working strain gauge, φ_{ref} is a signal from the reference resistance. The measurement bridge was energized by stabilized voltage from a power supply „Agat". An error of relative measurements of magnetostrictive strains did not exceed ±3 %.

Field dependences of longitudinal ($\lambda_{\parallel}$) and transverse ($\lambda_{\perp}$) magnetostriction were measured at the various temperatures. Volume magnetostriction of the studied samples was determined by the formula

$$\lambda_{\omega} = \lambda_{\parallel} + 2\lambda_{\perp}.$$

2. Results and discussion

Fig. 1 shows results of X-ray analysis of the rapidly-quenched samples of both the compositions $Tb_{0.2}Dy_{0.5}Gd_{0.3}Co_2$ and $Tb_{0.8}Dy_{0.1}Gd_{0.1}Co_2$. According to the XDA data, both the alloys are single-phase ones. In

Table 2. Structural and magnetic characteristics of the alloys $Tb_{0.2}Dy_{0.5}Gd_{0.3}Co_2$ and $Tb_{0.8}Dy_{0.1}Gd_{0.1}Co_2$

Compounds	a, nm	V, nm^3	T_C, K
$Tb_{0.2}Dy_{0.5}Gd_{0.3}Co_2$	0.7215	0.3755	248
$Tb_{0.8}Dy_{0.1}Gd_{0.1}Co_2$	0.7208	0.3745	243

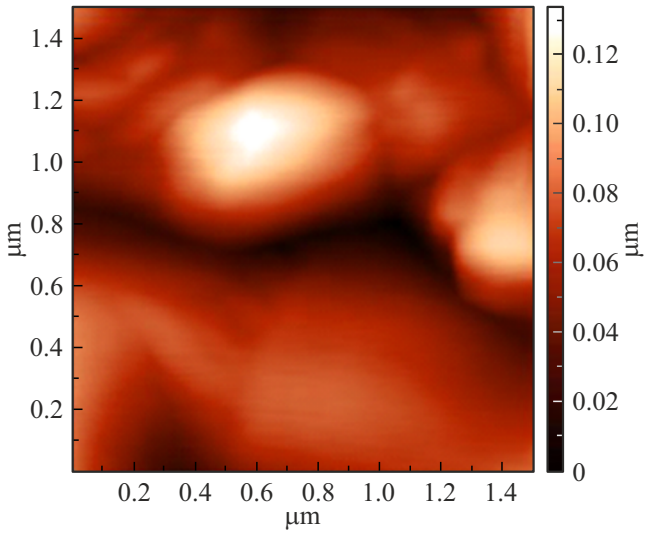

Figure 2. AFM photo of the cross section of the tape of the rapidly-quenched sample $Tb_{0.2}Dy_{0.5}Gd_{0.3}Co_2$.

spite the fact that the samples were rapidly quenched, the experimental X-ray spectra did not demonstrate presence of a plateau at small shooting angles and broadenings of diffraction peaks that indicate presence of an amorphous component. In other words, the structural state close to the optimally-quenched one was realized. Processing of the X-ray spectra resulted in determining values of the parameters of the crystal lattice of the rapidly-quenched samples $Tb_{0.2}Dy_{0.5}Gd_{0.3}Co_2$ and $Tb_{0.8}Dy_{0.1}Gd_{0.1}Co_2$, which are given in Table 2 together with calculated values of the volume of the crystal lattice. All the obtained data were comparatively analyzed to show that the composition and structural state did not significantly affect the value of these parameters. When varying the composition, the value of a relative change of the volume $\Delta V/V$ of the lattice cell was 0.27 %.

The AFM measurements were performed: 1) at a tapes' cross section (cleavage); 2) at the side that contacted a drum (the contact surface); 3) at the opposite side of the tape (the free surface). The studies were both in a micron scale and a nanoscale.

Fig. 2 exemplifies the AFM photos of the tape's cross section (the freshly prepared cleavage) of the rapidly-quenched $Tb_{0.2}Dy_{0.5}Gd_{0.3}Co_2$ sample (scanning by $1.5 \times 1.5\,\mu$m). It is clear that the cleavage of the $Tb_{0.2}Dy_{0.5}Gd_{0.3}Co_2$ sample is represented by structural elements of a various size and shape. It is found that the largest structural elements could have sizes of up to 5μm and usually consisted of finer structural elements.

The contact surface of both the samples $Tb_{0.2}Dy_{0.5}Gd_{0.3}Co_2$ and $Tb_{0.8}Dy_{0.1}Gd_{0.1}Co_2$ exhibited cracks oriented along one distinct direction. The sizes of the width and depth of the cracks varies from several micrometers to hundred nanometers. Cracking of the contact surface is related to melt crystallization on the copper water-cooled disk as a result of a sharp temperature gradient and large thermal stresses. Fig. 3 shows an AFM photo (scanning by $70 \times 70\,\mu$m) of the contact surface of the rapidly-quenched $Tb_{0.8}Dy_{0.1}Gd_{0.1}Co_2$ sample, which is made in the semi-contact mode. A height spread of heterogeneities was up to 2 μm. The same photos were obtained for another $Tb_{0.2}Dy_{0.5}Gd_{0.3}Co_2$ sample as well. All the obtained photos are analyzed to indicate that rapid quenching results in formation of a directional structure that is expressed in an ordered arrangement of the basic structural elements oriented strictly along a certain direction and that can significantly affect magnetostrictive properties of these alloys (see the text below).

The free surfaces of the multi-component Tb–Dy–Gd–Co alloys have been comparatively studied for their topography, defects, morphology of grains and conglomerates thereof in subsurface layers. We could not study grain boundaries since their width is as a rule below 10 nm. The cantilevers used by us had the tip rounding radius of 10 nm. Etching the boundaries by means of a concentrated acid solution would not have allowed obtaining a true surface picture and would result in fast formation of an oxide film on the surface as well.

Fig. 4, *a* shows the AFM image (scanning by $5.0 \times 5.0\,\mu$m) of morphology of the free surface of the $Tb_{0.2}Dy_{0.5}Gd_{0.3}Co_2$ sample. In order to identify specific

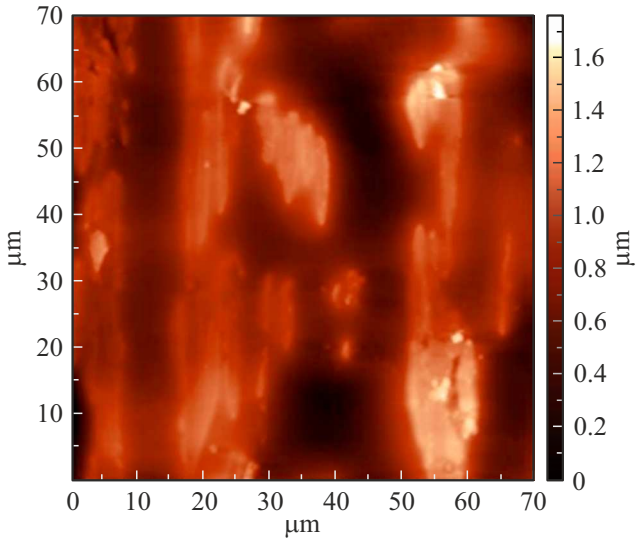

Figure 3. AFM photo of the contact surface of the tape of the rapidly-quenched sample $Tb_{0.8}Dy_{0.1}Gd_{0.1}Co_2$.

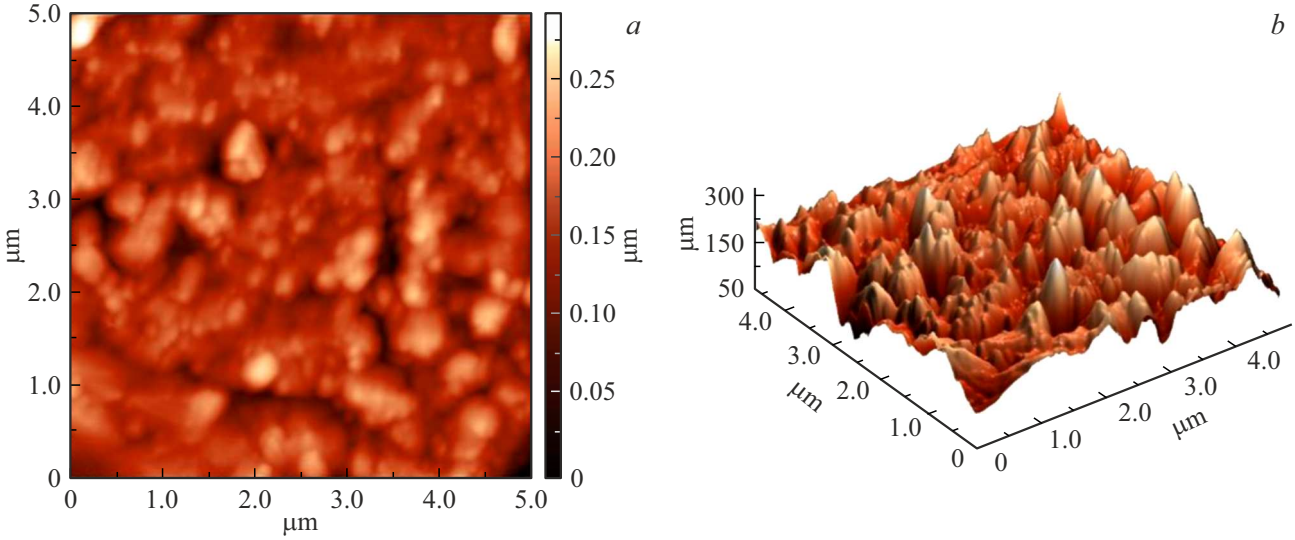

Figure 4. AFM photo (a) and 3D-image (b) of the free surface of the tape of the rapidly-quenched $Tb_{0.2}Dy_{0.5}Gd_{0.3}Co_2$ sample.

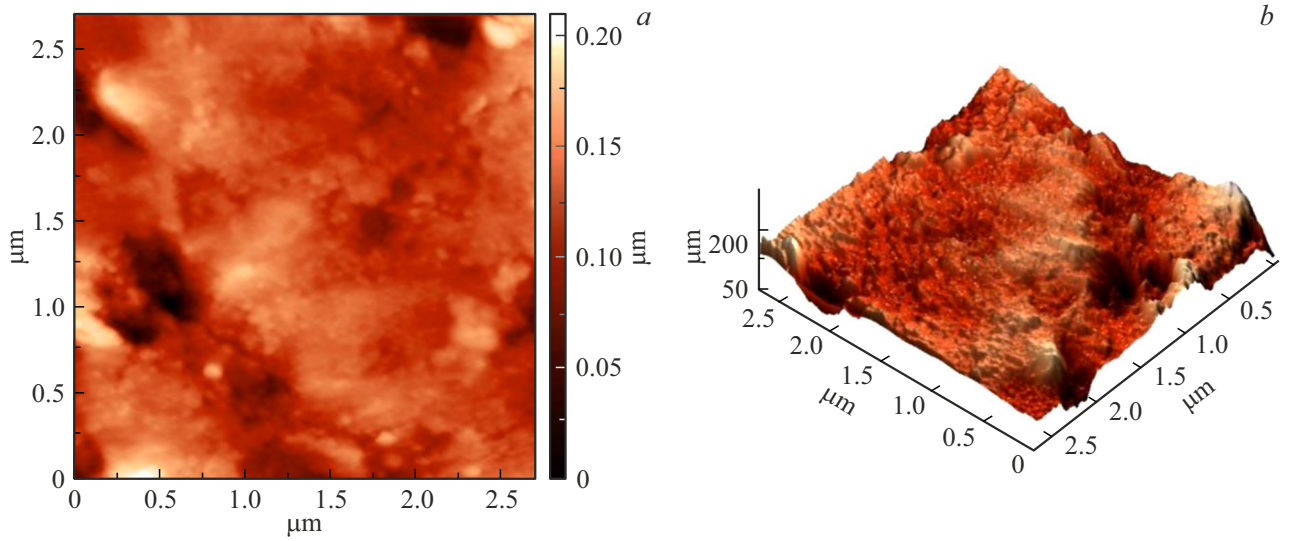

Figure 5. AFM photo ($2.7 \times 2.7\,\mu$m) (a) and 3D-image (b) of the free surface of the tape of the rapidly-quenched $Tb_{0.8}Dy_{0.1}Gd_{0.1}Co_2$ sample.

features of surface relief, Fig. 4, b shows a three-dimensional image of the surface. For comparison, Fig. 5 shows the AFM image (scanning by $2.7 \times 2.7\,\mu$m) of morphology of the free surface of the $Tb_{0.8}Dy_{0.1}Gd_{0.1}Co_2$ sample and the three-dimensional image of its surface, respectively.

The 3D images enable to see a difference of morphologies of the surface of the $Tb_{0.2}Dy_{0.5}Gd_{0.3}Co_2$ alloy and the $Tb_{0.8}Dy_{0.1}Gd_{0.1}Co_2$ alloy. The latter exhibits a smoother surface without large conglomerates and defects thereon. It is clear that the $Tb_{0.8}Dy_{0.1}Gd_{0.1}Co_2$ alloy with a high content of terbium consists of finer structural elements (grains) than the $Tb_{0.2}Dy_{0.5}Gd_{0.3}Co_2$ alloy. Previously, when studying morphology of the surface of high-purity rare-earth metals of terbium, dysprosium and gadolinium in the nanocrystalline state, which are produced as a result of procedures of distillation and sublimation, it was found that all of them had the grain size approximately from 200 to 300 nm [20]. For the rapidly-quenched four-component (Tb,Dy,Gd)Co_2 alloys studied herein, it is also possible to determine grain sizes by analyzing the AFM photos that are made also in the nanoscale scale.

Fig. 6, 7 shows the AFM photos of the $Tb_{0.2}Dy_{0.5}Gd_{0.3}Co_2$ alloys (scanning by $1.9 \times 1.9\,\mu$m) and the $Tb_{0.8}Dy_{0.1}Gd_{0.1}Co_2$ alloys (scanning by $1.0 \times 1.0\,\mu$m), which are taken at the nanolevel, and the profiles of sectioning the sample surface along the line S1. Fine structural elements are clearly visible in the photos. The section profile makes it possible to estimate sizes of these

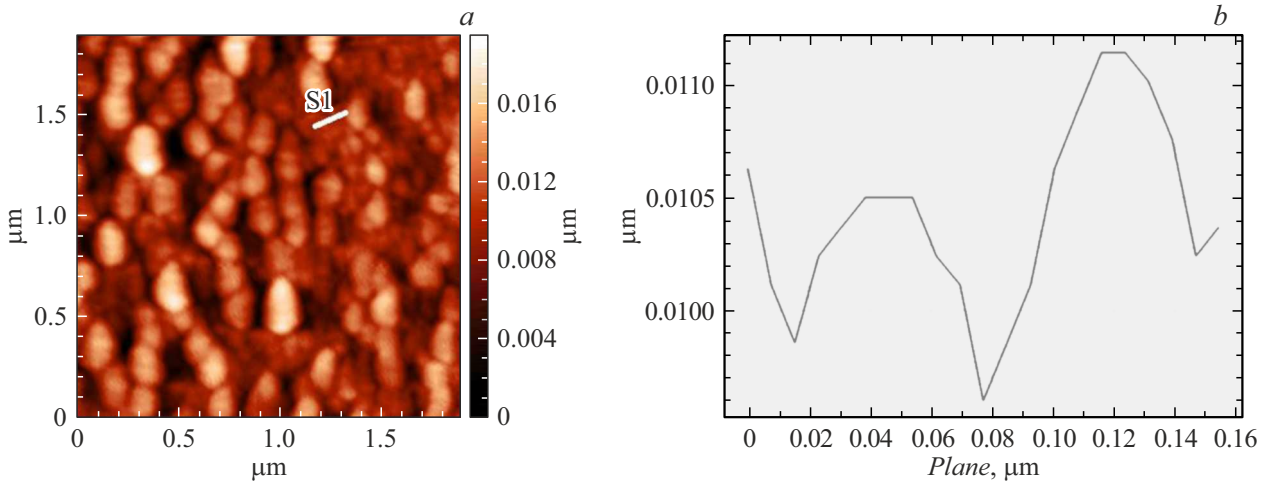

Figure 6. AFM image of morphology of the free surface (*a*) at the nanolevel and a profile of sectioning the sample surface along the line S1 (*b*) of the $Tb_{0.2}Dy_{0.5}Gd_{0.3}Co_2$ sample.

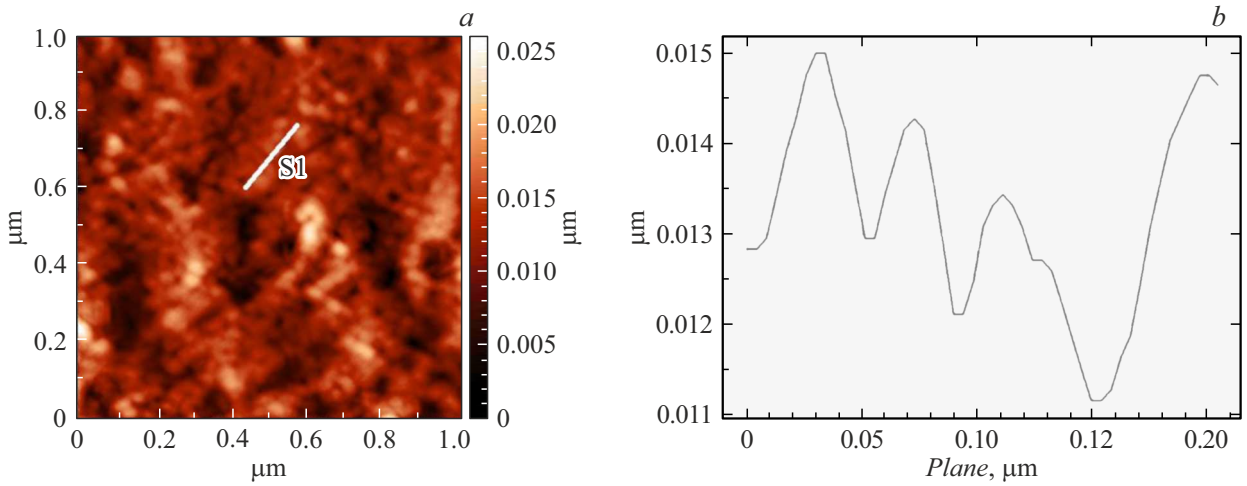

Figure 7. AFM image of morphology of the free surface at the nanolevel (*a*) and the profile of sectioning the sample surface along the line S1 (*b*) of the $Tb_{0.8}Dy_{0.1}Gd_{0.1}Co_2$ sample.

structural elements. It is found that the sizes of the finest structural elements are from 30 to 40 nm. At this, the structural elements are typical only for the composition with the high content of terbium, namely, $Tb_{0.8}Dy_{0.1}Gd_{0.1}Co_2$. With a decrease of the terbium content, the grain size increases in more than two times (80 – 100 nm). It should be noted changes happened not only to the size but to the shape of the grain as well: for $Tb_{0.8}Dy_{0.1}Gd_{0.1}Co_2$ the grain shape is oval, while for $Tb_{0.2}Dy_{0.5}Gd_{0.3}Co_2$ it is slightly elongated. Since both the samples were produced in the identical conditions, the observed phenomena could be related to specific features of rare-earth ions included in the composition of the alloys (Tb^{3+} and Dy^{3+} are highly-anisotropic ions, Gd^{3+} is an isotropic ion) and their content in the samples. We also note that the properties of the cast alloys of the $(Tb,Dy,Gd)Co_2$ system were also studied previously at the micro- and nano-level by means of AFM. The studies performed on a polished surface of the alloys made it possible to observe, for all the compositions, ovally-shaped grains, whose size exceeded the grain sizes of the rapidly-quenched samples and varied from 200 nm to 1 μm [21].

The present study also included investigation using a phase contrast, which did not identify presence of foreign phases on the surface of both the samples, thereby totally agreeing with the results of XDA on the powder samples.

As mentioned above, the alloys $Tb_{0.2}Dy_{0.5}Gd_{0.3}Co_2$ and $Tb_{0.8}Dy_{0.1}Gd_{0.1}Co_2$ can demonstrate significant magnetostrictive strains. Magnetostriction means variation of the sample sizes under effect of external magnetic fields. These size changes can be significant in value in the range of magnetic phase transitions, which include, as known, a transition of the „order-disorder“ type (the Curie temperature). The transitions of the „order-disorder“

type, i.e. spin-reorientation transitions, in which a magnetic moment of the compound in a jump-like manner (the first-order transition) or smoothly (the second-order transition) changes its position relative to crystallographic axes, are also accompanied by magnetostrictive strains [22,23]. Of particular interest was a comparative study of the magnetostrictive properties of the compounds $Tb_{0.2}Dy_{0.5}Gd_{0.3}Co_2$ and $Tb_{0.8}Dy_{0.1}Gd_{0.1}Co_2$ before and after rapid quenching in the temperature range near the Curie temperature with applying the external magnetic fields and taking into account the above-detected structural specific features. In these alloys, the Curie temperature (T_C) determined by means of thermomagnetic analysis was 248 and 243 K for $Tb_{0.2}Dy_{0.5}Gd_{0.3}Co_2$ and $Tb_{0.8}Dy_{0.1}Gd_{0.1}Co_2$, respectively (Table 2). We have not detected a significant difference in the values of the Curie temperature (taking into account a measurement error) for the rapidly-quenched and cast samples.

The temperature dependences of volume magnetostriction of the initial cast and rapidly-quenched $Tb_{0.2}Dy_{0.5}Gd_{0.3}Co_2$ alloy in the magnetic field of 12 kOe around the Curie temperature are shown in Fig. 8. It is clear that the curve $\omega(T)$ for the sample before rapid quenching is quite symmetric and demonstrates a maximum within the range of the temperatures close to the Curie temperature (which is typical for polycrystalline samples). A value of the maximum is $0.25 \cdot 10^{-3}$ when $T = T_{\max}$. High values of magnetostrictive strains are preserved in a quite wide range of the temperatures ($\Delta T = T_2 - T_1 = 15$ K). For the sample after rapid quenching, a type of the curve $\omega(T)$ is significantly changed: its symmetry is broken and it exhibits a pronounced maximum. The value of the maximum is $0.295 \cdot 10^{-3}$. The temperature range, in which these high values are realized, is significantly narrowed. This type of the curve is usually typical for single-crystal samples or pseudo-single-crystal samples. Creating the directional structure in the samples by means of rapid quenching makes it possible to obtain higher values of volume magnetostriction: the increase is about 20 %.

It is well known that the rapidly-quenched alloys form a typical directional structure, which is essentially different from a structure of coarsely-crystalline samples. Structure directivity reflects anisotropy in the shape, size, orientation of grains and/or quasi-crystalline areas and it originates due to fast cooling and limited time for diffusion processes and recrystallization. The main parameter of structure directivity can take into account the shape, size, orientation of not only the grains, but the quasi-crystalline areas and their distribution. We note that in the studied rapidly-quenched alloys the grain shape does not differ much from the grain shape in the cast samples. At the same time, the formed separate quasi-crystalline areas had preferable orientation relative to a disk rotation direction, which generally resulted in their directional ordering. Anisotropy caused by the directional structure (induced anisotropy) contributes to redistribution of magnetic domains, variation of magnetic interactions and local internal stresses. At

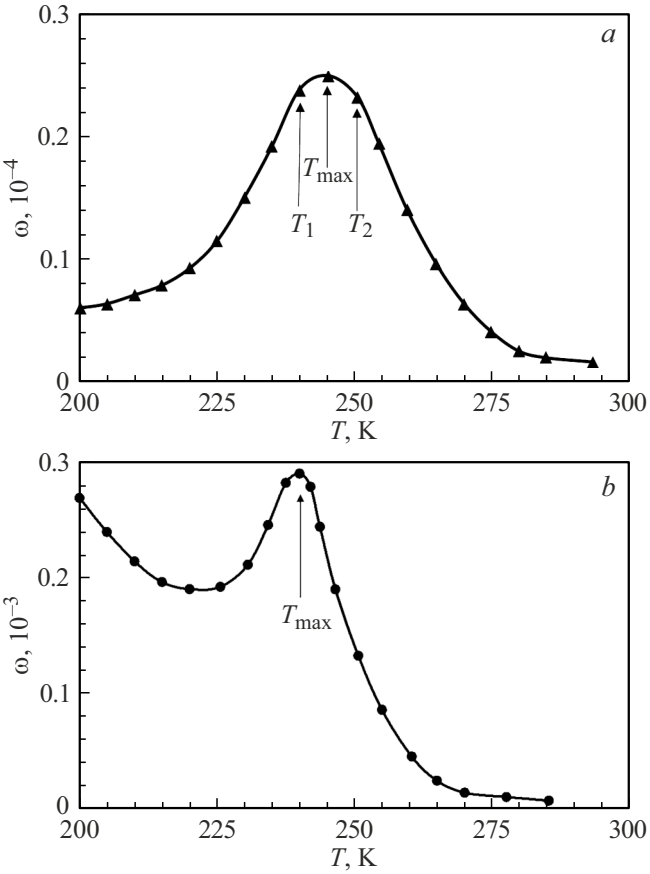

Figure 8. Temperature dependences of volume magnetostriction of the initial (*a*) and rapidly-quenched (*b*) $Tb_{0.2}Dy_{0.5}Gd_{0.3}Co_2$ alloy in the magnetic field of 12 kOe.

the same time, there is usually an increase of sensitivity (enhancement/attenuation) of magnetostrictive strains to the external magnetic field.

The above-observed increase of magnetostriction occurs with complete absence of an amorphous phase in the samples (which was shown by X-ray studies) as well as when the rapidly-quenched alloys have the quasi-crystalline oriented areas, whose length exceeds 20 μm (Fig. 3), and nanograins of the size of up to 100 nm (which are detected by means of AFM (Fig. 6 and 7)).

Now we demonstrate which basic mechanism can be responsible for high magnetostrictive characteristics of the studied alloys. As it is clear from Table 2, varying the composition in the (Tb,Dy,Gd)Co_2 system results in a change of the Curie temperature and a volume of the lattice cell. It has been previously shown in the studies [24–26] for the Fe-containing compounds with the structure of the Laves phases $Tb_{0.3}Dy_{0.7}Fe_2$ (Terfenol — D), YFe_2 and their hydrides that when the volume of their lattice cells is changed α — a change of the integral of exchange interaction A

$$\alpha = \frac{d \ln A}{d \ln V} = \frac{d \ln T_C}{d \ln V}$$

has a value that is close to 3 (in modulus). The Curie temperature in the RFe_2 compounds is mainly contributed by exchange interactions in the pairs Fe–Fe. As a result, substitution of non-magnetic Y with magnetoactive ions of terbium and dysprosium has not significantly affected the magnitude α. In the compounds of the RCo_2 type, the situation is somewhat different: the YCo_2 compound does not exhibit magnetic ordering within the entire temperature range and is an exchange-enhanced Pauli paramagnetic. The magnetic-ordered state in YCo_2 can be realized under effect of the strong magnetic field (of about 700 kOe [27]) and as a result of partial or full substitution of Y with magnetoactive rare-earth metals as well. That is why exchange interactions in the pairs Co–Co can not dominantly contribute to the Curie temperature of the RCo_2 compounds. Intersublattice exchange interactions of R–Co prevail over exchange interactions in the pairs Co–Co and R–R. Using the formula

$$\Delta T_C = T_C \cdot \frac{\Delta V}{V} \cdot \frac{d \ln T_C}{d \ln V},$$

one can obtain the value of α, which, in our estimates, is 7.7. The value of α obtained for our studied multi-component $(Tb,Dy,Gd)Co_2$ compounds with good accuracy coincides with the value of α for the binary $TbCo_2$ compound, which is given in the study [28], in which the samples are subjected to hydrostatic pressure. Thus, it can be concluded that the compounds of the RCo_2 type can demonstrate high values of volume magnetostriction around the Curie temperature due to a sharp dependence of the resultant integral of exchange interaction on the volume of the lattice cell (the „volume“ effect). The change of the volume of the lattice cell $\frac{\Delta V}{V}$ is directly related to variation of the distances in the pairs R–Co, Co–Co and R-R. This change is possible not only under effect of hydrostatic pressure, but also when replacing rare-earth atoms with the others due to, in particular, a phenomenon of lanthanide compression.

Around the Curie temperature, the compounds of the RCo_2 type can demonstrate high values of not only magnetostriction, but another most important effect, i.e. the magnetocaloric effect [28–30]. Using one or, simultaneously, two effects as well as producibility of the tape-shaped nanostructured samples can significantly extend ranges of application of these materials, for example, in robotics or medical equipment.

Conclusion

Investigation of the nanoscale-grain materials requires to use the most modern and, as a rule, comprehensive approach. Formation of the nanocrystalline structure can play a special role when forming physical properties. At the same time, it is very important to understand the basic mechanisms of its formation and effect on these properties.

The study has demonstrated efficiency of the AFM method for studying the nanostructured multi-component $(Tb,Dy,Gd)Co_2$ alloys in the micro- and nano-scale range along with other experimental (X-ray diffractometry, magnetometry) and computational methods. The AFM studies and XDA of the two rapidly-quenched $Tb_{0.2}Dy_{0.5}Gd_{0.3}Co_2$ and $Tb_{0.8}Dy_{0.1}Gd_{0.1}Co_2$ samples were at the room temperature. It is found that both the samples completely lacked the amorphous phase and structural parameters of the alloys have been determined. For the multi-component $(Tb,Dy,Gd)Co_2$ alloys, we have obtained important information about topography of the cleavages, the contact and free surfaces of the tape samples, morphology of the nanograins in the subsurface layers, the sizes of the basic structural elements, which affect the functional properties.

The surfaces of both the rapidly-quenched samples that are produced in the identical conditions demonstrated nanoscale relief. The sizes of the finest structural elements (grains) were $30 - 40$ nm. These structural elements were typical only for the composition with the high content of terbium, namely, $Tb_{0.8}Dy_{0.1}Gd_{0.1}Co_2$. With a decrease of the Tb content, we observed a double increase of the grain size in the composition $Tb_{0.2}Dy_{0.5}Gd_{0.3}Co_2$. The AFM images of the contact surface of both the samples were analyzed to demonstrate that the directional structure was formed in them as a result of rapid quenching. It resulted in an increase of the value of volume magnetostriction around the Curie temperature by 20% as compared to magnetostriction of the initial cast samples. The high values of magnetostrictive strains are generally caused by the volume effect that is related to a quite strong dependence of exchange integrals on the volume of the lattice cell. It significantly extends the prospects for practical use of the RCo_2 compounds, whose functional properties can be increased as a result of formation of the nanocrystalline structure in them.

Funding

This study was performed under the state assignment of the M. V. Lomonosov Moscow State University.

Conflict of interest

The authors declare that they have no conflict of interest.

References

[1] F. Stein, A. Leineweber. J. Mater. Sci., **56**, 5321 (2021). DOI: 10.1007/s10853-020-05509-2
[2] E. Gratz, A.S. Markosyan. J. Phys. Condens. Matter, **13**, 385 (2001). DOI: 10.1088/0953-8984/13/23/202
[3] S. Khmelevsky, P. Mohn. J. Phys. Condens. Matter, **12**, 9453 (2000). DOI: 10.1088/0953-8984/12/45/308
[4] N.H. Duc, T. Goto. In: *Handbook on Physics and Chemistry of Rare Earths*, ed. by K.A. Gschneidner, Jr., LeRoy Eyring (Elsevier Science, Amsterdam, 1999), v. 26, p. 177.
[5] N.H. Duc, D.T. Kim Anh, P.E. Brommer. Phys. B: Condens., **319**, 1 (2002). DOI: 10.1016/S0921-4526(02)01099-2

[6] M.S. Anikin, E.N. Tarasov, N.V. Kudrevatykh, A.A. Inishev, A.V. Zinin. Metal Sci. Heat Treatment, **60**, 7 (2018). DOI: 10.1007/s11041-018-0312-4
[7] G.A. Politova, V.B. Chzhan, I.S. Tereshina, G.S. Burkhanov. Phys. Solid State, **57**, 2417 (2015). DOI: 10.1134/S1063783415120288
[8] D.A. Morozov, G.A. Politova, M.A. Ganin, M.E. Politov, A.B. Mikhailova, A.V. Filimonov. Phys. Metals Metallography, **125**, 393 (2024). DOI: 10.1134/S1063783414090224
[9] C. Zhou, K. Li, Y. Chen, Z. Dai, Y. Wang, L. Wang, Y. Matsushita, Y. Zhang, W. Zuo, F. Tian, A. Murtasa, S. Yang. Materials, **15**, 3884 (2022). DOI: 10.3390/ma15113884
[10] I.S. Tereshina, V.B. Chzhan, E.A. Tereshina, S. Khmelevskyi, G.S. Burkhanov, A.S. Ilyushin, M.A. Paukov, L. Havela, A.Yu. Karpenkov, J. Cwik, Yu.S. Koshkid'ko, M. Miller, K. Nenkov, L. Schultz. J. Appl. Phys., **120**, 01390 (1) (2016). DOI: 10.1063/1.4955047
[11] W. Luo, C. Kirchlechner, J. Zavašnik, W. Lu, G. Dehm, F. Stein. Acta Mater., 2020. DOI: 10.1016/j.actamat.2019.11.036
[12] J. Eckert, A. Reger-Leonhard, B. Weiss, M. Heilmaier, L. Schultz. Adv. Eng. Mater., **3**, 41 (2001). DOI: 10.1002/1527-2648(200101)3:1/2<41::AID-ADEM41>3.0.CO;2-S
[13] I.A. Pelevin, I.S. Tereshina, G.S. Burkhanov, S.V. Dobatkin, T.P. Kaminskaya, D.Yu. Karpenkov, A. Zaleski, E.A. Tereshina. Phys. Solid State, **56**, 1778 (2014). DOI: 10.1134/S1063783414090224
[14] L. Shultz. In: *Science and technology of nanostructured magnetic materials*, ed. by G.C. Hadjipanayis, G.A. Prinz (Springer, 1990), v. 259, p. 583. DOI: 10.1007/978-1-4899-2590-9_65
[15] O. Gutfleisch, M.A. Willard, E. Brück, C.H. Chen, S.G. Sankar, J.P. Liu. Adv. Mater., **23**, 821 (2011). DOI: 10.1002/adma.201002180
[16] M.D. Coey. *Magnetism and Magnetic Materials* (Cambridge University Press, Cambridge, 2010)
[17] V.L. Mironov. *Osnovy skaniruyushchei zondovoi mikroskopii* (In-t fiziki mikrostruktur RAN, 2004) (in Russian).
[18] V.M. Grabov, E.V. Demidov, V.A. Komarov. Phys. Solid State, **50** (7), 1312 (2008). DOI: 10.1134/S1063783408070287
[19] G.S. Burkhanov, I.S. Tereshina, G.A. Politova, O.D. Chistyakov. Dokl. Phys., **56** (10), 513 (2011). DOI: 10.1134/S1028335811100065
[20] Yu.V. Korneeva, V.B. Chzhan, I.S. Tereshina, T.P. Kaminskaya, E.A. Tereshina-Chitrova, H. Drulis, K. Rogacki. Int. J. Hydrogen Energy, **46** (27), 14556 (2021). DOI: 10.1016/j.ijhydene.2021.01.228
[21] G.A. Politova, G.S. Burkhanov, I.S. Tereshina, T.P. Kaminskaya, V.B. Zhang, E.A. Tereshina. J. Tech. Phys., **87** (4), 557 (2017). DOI: 10.21883/JTF.2017.04.44316.1995
[22] K.P. Belov. *Magnitostriktsionnye yavleniya i ikh tekhnicheskie prilozheniya* (Nauka, M., 1987) (in Russian).
[23] A.S. Ilyushin. *Osnovy strukturnoi fiziki redkozemel'nykh intermetallicheskikh soedinenii* (MGU, M., 2005) (in Russian).
[24] S.A. Nikitin. Vestnik Moskovskogo un-ta. Seriya 3: Fizika, astronomiya **6**, 27 (2011) (in Russian).
[25] A.A. Aleroev, I.S. Teryoshina, T.A. Aleroeva, N.Y. Pankratov, S.A. Nikitin. Solid State Physics, **66** (8), 1378 (2024). DOI: 10.61011/FTT.2024.08.58603.156
[26] S.A. Nikitin, N.Y. Pankratov, A.I. Smarzhevskaya, G.A. Politova, Y.G. Pastushenkov, K.P. Skokov, A. del Moral. J. Appl. Phys., **117**, 193908 (2015). DOI: 10.1063/1.4919593
[27] T. Goto, K. Fukamishi, T. Sakakibara, H. Komatusu. Solid State Commun., **72**, 945 (1989).
[28] M. Brouha, K.H.J. Buschow, A.R. Miedema. IEEE Transactions on Magnetics, MAG-10, 82 (1974).
[29] A.M. Tishin, Y.I. Spichckin. *The Magnetocaloric Effect and its Applications* (Institute of Physics Publishing, Bristol, 2003)
[30] G.A. Politova, I.S. Tereshina, J. Cwik. J. Alloys Compd., **843**, 155887 (2020). DOI: 10.1016/j.jallcom.2020.155887
[31] V.B. Chzhan, I.S. Tereshina, A.Yu. Karpenkov, E.A. Tereshina-Chitrova. Acta Mater., **154**, 303 (2018). DOI: 10.1016/j.actamat.2018.05.053

Translated by M.Shevelev